Brazilian Journal of Geophysics (2021) 39(4): 565–583
© 2021Brazilian Geophysical Society
ISSN 2764-8044
DOI 10.22564/rbgf.v38i4.2113

ASSESSMENT OF TWO REFRACTION TRAVELTIME TOMOGRAPHY METHODS APPLIED FOR STATICS CORRECTIONS OF LAND DATA

Bruno Freitas Gonçalves [1,2] and German Garabito Callapino [3]

ABSTRACT. Many refraction tomography algorithms for statics corrections have model parameterization, forward modeling, and inversion limitations. For instance, most traditional methods use a regular grid to parameterize the model and only invert one parameter, either velocity or thickness of the layer. Generally, these conventional techniques do not allow the simultaneous inversion of traveltimes of turning-rays and head-waves either. In this study, for the first time, we applied and evaluated the well-known 2D refraction tomography algorithm Rayinvr, which is widely used to study deep crustal models, to estimate near-surface layered velocity models and static corrections from real seismic reflection data collected for oil exploration. Here, the Rayinvr and its results are compared with another refraction tomography algorithm widely used in the petroleum industry. It employs the concept of generalized linear inversion and uses a simplified earth model composed of a layer over a half-space, which is parameterized by vertical rectangles of constant velocity. The results of both methods were applied and evaluated on two real datasets of seismic lines located in Brazilian onshore basins. The Rayinvr tomography algorithm provides precise measurement statics corrections, better velocity models, and more reliable geological structures than the standard tomography algorithm.

Keywords: refraction, seismic tomography, traveltimes, near-surface geophysics

RESUMO. Muitos algoritmos de tomografia de refração para correções estáticas têm limitações em relação à parametrização do modelo, da modelagem direta e da inversão. Por exemplo, a maioria dos métodos tradicionais usa uma malha regular para parametrizar o modelo e apenas invertem um parâmetro, seja a velocidade ou a espessura da camada. Geralmente essas técnicas convencionais também não permitem a inversão simultânea dos tempos de trânsito de *turning-rays* e *head-waves*. Neste estudo, pela primeira vez, aplicamos e avaliamos o conhecido algoritmo de tomografia de refração 2D Rayinvr, que é amplamente usado no estudo de modelos crustais profundos, na estimativa de modelos de velocidade em camadas próximas à superfície e nas correções estáticas de dados reais de reflexão sísmica coletados para exploração de petróleo. Aqui, o Rayinvr e os resultados são comparados com outro algoritmo de tomografia de refração, amplamente utilizado na indústria petrolífera. Ele emprega o conceito de inversão linear generalizada e usa um modelo terrestre simplificado composto por uma camada sobre um meio-espaço, que é parametrizado por retângulos verticais de velocidade constante. Os resultados de ambos os métodos foram aplicados e avaliados em dois conjuntos de dados reais de linhas sísmicas localizadas em bacias terrestres brasileiras. O algoritmo de tomografia Rayinvr forneceu correções estáticas mais precisas, melhores modelos de velocidade e estruturas geológicas mais confiáveis do que o algoritmo padrão de tomografia.

Palavras-chave: refração sísmica, tomografia sísmica, tempos de trânsito, geofísica rasa

Corresponding author: Bruno Freitas Gonçalves

[1] Petróleo Brasileiro S. A., Rio de Janeiro, RJ, Brazil
[2] Universidade Federal do Rio Grande do Norte (UFRN), Programa de Pós-graduação em Ciência e Engenharia do Petróleo (PPGCEP), Natal, RN, Brazil – E-mail: brunofreitasgoncalves@gmail.com
[3] Universidade Federal do Rio Grande do Norte (UFRN), Departamento de Engenharia do Petróleo (DPET) Natal, RN, Brazil – E-mail: germangca@gmail.com

INTRODUCTION

Land seismic reflection data are typically acquired on an uneven surface (topography), where the topmost superficial layer, commonly referred to as the low-velocity layer (LVL), is composed of weathered material with low seismic velocity propagation. Variations in the physical properties of this upper layer can cause a dramatic deterioration in the land seismic data quality. Seismic arrival times from source to receivers undergo time shifts that depend on the acquisition geometry, topography, velocity, and depth of near-surface layers.

In land seismic reflection for oil exploration, the presence of the near-surface low-velocity layer can degrade the image of the deeper structures. Lateral variations in the thickness or velocity of the weathering layer can corrupt the continuity of reflection events on the stacked section or migrated image. Furthermore, when the near-surface effects are not appropriately corrected by static correction, apparent structures can be inserted into deep reflectors. Refraction tomography has proved to be valuable for obtaining the near-surface information required for static corrections to overcome this problem (Marsden, 1993).

The most common refraction tomography methods are based on prism parameterization, which generally suffers from a velocity–depth trade-off. To circumvent this ambiguity, Hampson and Russell (1984) solved the weathering thickness by assuming that the velocity information is known, via a *generalized linear inversion* method, while Olsen (1989) introduced an identical *inverse modeling* method. Similarly, Amorim *et al.* (1987) solved the weathering velocity through a *numerical equivalent* method, wherein the thickness information is assumed to be known. In all these approaches, the model is parameterized in vertical rectangles, an input model is designed using a standard refraction interpretation, and theoretical first break traveltimes are computed. The model is then perturbed iteratively until the computed and observed traveltimes match the squared-error criterion.

The methods mentioned above use straight-ray approximation and do not allow a vertical velocity gradient. To handle media with a vertical velocity variation, Zhu *et al.* (1992) and Stefani (1995) introduced the *turning-ray tomography method*. In this method, the ray propagation allows curved-rays and, therefore, a vertical velocity gradient. In regions where head-waves cannot be easily identified as refractors, this method has advantages. The turning-ray tomography method employs a parameterization of uniform grids, and therefore requires many parameters for inversion. If not handled appropriately, the result can become unstable. In general, this method does not allow the use of joint turning and straight-rays, which can be useful in regions where the refractor is well defined by head-waves (straight-rays) and the LVL layer has a vertical velocity gradient (turning-rays). An exception can be found in Boehm *et al.* (2012), where they jointly invert the traveltimes both associated to diving-waves (by turning-rays) and to head-waves, by using the method of *minimum dispersion of reflected/refracted points* to detect the shape and the depth of the refractor and using the crossover points to separate the diving-wave arrivals from the head-wave ones.

Zelt and Ellis (1988) and Zelt and Smith (1992) introduced a tomographic inversion algorithm to determine the velocity model and crustal structure. Called Rayinvr, this algorithm uses a model with interfaces that form segmented layers defined by trapezoids. The computational cost is low because it does not use uniform grids. Furthermore, the use of interfaces allows flexibility in the model construction, as the vertices of the trapezoids do not need regular sampling. This parameterization of the model also enables vertical and lateral velocity gradients within the layers. This algorithm allows the combination of layers with constant velocity and velocity gradient, thus facilitating the inversion of more general models than the standard refraction tomography methods applied for static corrections.

The algorithm has been used in several studies for modeling and inversion of deep crustal structures (Bauer *et al.*, 2000; Dean *et al.*, 2000; Gutscher *et al.*, 2002). However, there are some applications for shallow modeling and inversion studies. For example, Ogunsuyi and Schmitt (2012) applied Zelt's program to estimate a new surface velocity model to highlight materials that make up the paleo-valley of other surrounding rock bodies in a survey of high-resolution seismic reflection. Talukdar and Behera (2018) used the algorithm to aid in imaging complex underground geological structures beneath a highly heterogeneous and thick column of rough basalt layers. It is important to highlight the lack of application of the Rayinvr algorithm for shallow refraction tomography and statics corrections of the seismic reflection data acquired for oil exploration.

Ray-tracing traveltime tomography, a high-frequency approximation, sometimes fails to compute Fréchet derivatives due to shadow zones. In order to overcome this weakness, a *wave-equation traveltime tomography* was developed (Luo and Schuster, 1991). This method can describe high velocity-contrast models but it incurs high computational costs to compute wavepaths. However, other methods were develop to reduce the computational costs (Schuster and Quintus-Bosz, 1993; Pyun *et al.*, 2005).

Seismic tomography methods that use *early arrival waveform inversion* were developed (Sheng *et al.*, 2006; Shen, 2010). These methods estimate velocity by recorded early arrivals based on the finite-frequency wave equation. They naturally consider more general wave-propagation effects compared to the high-frequency method of traveltime tomography, meaning that early waveform tomography can estimate a wider range of slowness wavenumbers (Sheng *et al.*, 2006). However, these methods can be computationally more expensive, suffer with lack of quality of the waveform from real data and, depending on the size of the grid,

suffer with instability, compromising the final inversion results.

A layer-based algorithm called *deformed layer tomography* (DLT) method (Zhou, 2006), using the multiscale regularization strategy, can be a particularly robust solution, specially when velocity values are known in parts of the model or the inversion is restricted in parts of the model (Zhou *et al.*, 2009). In DLT method, model parameterization consists of layers represented by triangular prisms and, in areas with good ray coverage, can be used to invert the layer interval velocities and interface geometry simultaneously. This tomographic method can also be used to solve shallow models with velocity inversion, where most refraction tomography methods fail (Liu *et al.*, 2010). However, this method does not work with lateral velocity variations and vertical velocity gradients within the layer, only with homogeneous values of interval velocity. According to Zhou (2006), to consider lateral and vertical velocity variations, it is necessary to isolate the structural kernel from the velocity one in separate inversions.

Gonçalves and Garabito (2021) applied Rayinvr seismic refraction tomography from Zelt and Smith (1992), adapted to determine shallow structural and velocity models from reflection data. The algorithm was validated using two synthetic data generated from models that represent different heterogeneous weathering zones. They called this a *flexible layer-based tomography* and inverted multiple model parameters (both depth and velocity) and compared the results with the delay time method, obtaining good inverted model parameters and statics correction results.

In this work, we present a pioneering assessment study of the Rayinvr tomography algorithm to determine the near-surface layered structure and the velocity model from real land seismic reflection data acquired for oil exploration, and then we calculate statics corrections. A new methodology developed to estimate the initial velocity model required to apply the refraction tomography with Rayinvr will be applied in real data. The Rayinvr algorithm is applied in two real datasets from seismic lines localized in Brazilian onshore basins. For the first seismic line, the model contains vertical gradient in the LVL and variable lateral velocity for the refractor. Therefore, for Rayinvr tomography, turning-rays through the LVL layer are considered in the inversion process. For the second seismic line, a model was used with two refractors separating layers with lateral velocity variations. In order to compare the results of the Rayinvr, a proprietary software called Refratom, which uses a model solution called *numerical equivalent* for refraction tomography (Amorim *et al.*, 1987), is applied to the same two real datasets.

2D FIRST-ARRIVAL TRAVELTIME TOMOGRAPHY METHODS

This section briefly describes both tomographic refraction methods used in this study. First, the estimated model parameters, i.e., thickness and velocity of the near-surface using these tomography methods, are used to correct seismic data for medium- to long-wavelength static anomalies caused by variations in topography, weathering layer, and refractors. After applying the static field corrections to the seismic shot and receiver records, the data are repositioned to a *floating datum*, calculated by an average of the statics. The data positioned in the *floating datum* are corrected for high frequency statics and will be close to the acquisition surface, which will not affect subsequent velocity and migration analysis procedures.

Table 1 provides an objective comparison between turning-ray tomography, Refratom and Rayinvr algorithms. Several parameters are different; the main ones being model parameterization, ray tracing, type of arrival, inverted parameters and vertical velocity variation. Despite being shown in this comparative table, the turning-ray tomography was not used in this work.

The benefit of turning-ray tomography is that it makes no assumptions regarding the existence or geometry of layers in the near-surface and, consequently, it performs well not only when the near-surface geometry/velocity is very complex but also when it is characterized by simple layering. However, the associated cost is that the velocity inversion must smooth through areas of abrupt velocity change, such as the transition from the weathering layer to the top of a fast refractor (Stefani, 1995).

If the subsurface were known to be characterized by hard-rock layering with a strong velocity contrast and without complicated pinchouts or low-velocity zones in depth, then a conventional refraction technique should probably be used for the best possible resolution. In this sense, Refratom and Rayinvr methods should work well. Despite that, Rayinvr can use the best of both methods, which use straight and curved rays, work with layers and can invert velocity and depth simultaneously. Rayinvr's biggest limitation would be its geometry, which only allows 2D data. However, its flexibility, in parameterization, modeling and inversion, shows significant advantages over Refratom.

RAYINVR

Zelt and Smith (1992) developed a technique for inverting traveltimes to obtain simultaneously 2D velocity and interface structure, in which the model parameterization and ray-tracing method are suitable for the forward step of an inversion algorithm. The method is applicable to any set of traveltimes for which forward modeling is possible, regardless of the shot–receiver surface geometry. The traveltime inversion non-linearity makes necessary a starting model and iterative approach, thus requiring a practical and efficient forward step.

The model parameterization consists of fragmented layer interfaces formed by an irregular network of trapezoids. In this study, the model was constructed using trapezoids with regular width, corresponding to the interval between receivers or their multiple values, each

Table 1. Features of Turning-ray, Refratom and Rayinvr seismic tomography algorithms. *This is dependent on the complexity of the ray tracing algorithm implemented in the inversion procedure. If one uses SIRT (Simultaneous Iterative Reconstruction Technique), as an inversion method, the model can be defined also by irregular grid.

Features	Turning-ray	Refratom	Rayinvr
Model parameterization	Rectangular grid*	Vertical prisms	Vertical trapezoids
Sampling of parameters	Regular*	Regular	Regular or irregular
Ray tracing	Curved	Straight	Straight and/or Curved
Seismic arrival	Turning-rays	Head-waves	Reflection, Head-waves, Turning-rays
Allow multiple arrival?	No	No	Yes
Inverted parameters	Velocities	Only V_0	Velocities and/or depths
Lateral velocity variation	Yes	Yes	Yes
Vertical velocity variation	Yes	No	Yes
Number of layers	NA	Two	No limits
Work with uncertainties?	No	No	Yes
Work with regularization?	Yes	No	Yes

of which forms part of the upper and lower boundaries of the layer. The velocities at the four corners of the trapezoid were used to interpolate a velocity field that varies linearly along its four sides. Therefore, horizontal and vertical velocity gradients may exist within a trapezoid. The number and position of the model parameters (velocity and interface nodes), which specify each layer, can be completely general and adapted to the subsurface data resolution. The algorithm also allows topography and near-surface velocity variations to be incorporated into the model. Figure 1 shows an example for near-surface model parameterization with three layers. In this example, note that (1) the node positions on the surface model do not invert, but still break the first layer in 48 blocks; (2) the first layer has a vertical and lateral velocity gradient; (3) the second layer only has lateral velocity variation; (4) the third layer has a constant velocity; (5) despite being shown as equispaced, the node points can have variable spacing, both for depth and velocity nodes.

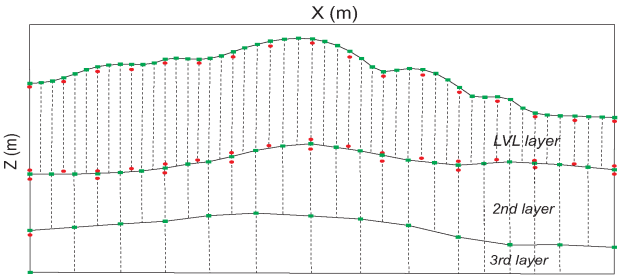

Figure 1. Example of near-surface velocity model parameterization for refraction tomography in Rayinvr. The three-layer model is defined by 132 independent model parameters: 88 boundary nodes (green squares) and 44 velocity points (red circles). For ray tracing, the model is automatically divided into 84 trapezoidal blocks.

Initially, for forward modeling, ray take-off angles of particular ray groups are determined using an iterative shooting/bisection technique (Zelt and Ellis, 1988; Zelt and Smith, 1992). Then rays are traced through the velocity model using the zero-order asymptotic ray theory by solving the ray-tracing equations numerically (Cerveny *et al.*, 1977). The 2-D ray-tracing equations constitute a pair of first-order ordinary differential equations. The ray-tracing system is solved with x as the integration variable when the ray path is near-horizontal or with z as the integration variable when the ray path is near-vertical (where "x" represents the horizontal direction, and "z" the vertical direction). The Runge–Kutta method (Sheriff and Geldart, 1983) with error control is used to solve these systems, as Cerveny *et al.* (1977) suggested. Finally, Snell's law is applied at the intersection of a ray with a layer boundary to complete the basic ray-tracing algorithm.

A smoothed damped least-square inversion — Eq. (1) — is used to determine the updated model parameters of those selected for adjusting both the velocity and boundary nodes simultaneously (Zelt and Smith, 1992; Gonçalves and Garabito, 2021):

$$\Delta\mathbf{m} = \left[\mathbf{A}^{\mathbf{T}}\mathbf{C}_{\mathbf{t}}^{-\mathbf{1}}\mathbf{A} + \lambda\mathbf{D}^{\mathbf{T}}\mathbf{C}_{\mathbf{m}}^{-\mathbf{1}}\mathbf{D}\right]^{-1}\mathbf{A}^{\mathbf{T}}\mathbf{C}_{\mathbf{t}}^{-\mathbf{1}}\Delta\mathbf{t} \quad (1)$$

where $\mathbf{A}$ is the partial derivative matrix (also called Frechèt derivatives), $\Delta\mathbf{t}$ is the residual vector of the traveltime, and $\Delta\mathbf{m}$ is the unknown model parameter perturbation that needs to be determined. The partial derivative matrix contains the elements $\partial t_i/\partial m_j$, where t_i is the ith observed traveltime and m_j is the parame-

ter of the jth model selected for the inversion, for the velocity value or the z coordinate of a boundary node. Parameter $\mathbf{D}$ is Tikhonov regularization operator; $\mathbf{C_t}$, and $\mathbf{C_m}$ are the estimated data and model covariance matrices given by $\mathbf{C_t} = diag(\sigma_i^2)$ and $\mathbf{C_m} = diag(\sigma_j^2)$; σ_i is the standard deviation related to an estimated uncertainty of the traveltime i; σ_j is the standard deviation related to an *a priori* estimated uncertainty of the model parameter j; and λ is an overall damping and smoothing parameter.

The Tikhonov regularization operator $\mathbf{D}$ employs a first derivative of model parameters and is used to enforce smoothness of the solution. This operator improves the conditioning of the problem, that is, transforms an ill-posed problem into a well-posed one, thus enabling a direct numerical solution. The relative values of σ_v and σ_z, determine the *trade-off* between the parameter size and the contour adjustments in the inversion. The parameter λ is a positive constant called the *regularization factor* which represents the intensity of the regularization applied to obtain a satisfactory solution. The value of λ determines the overall *trade-off* between the resolution and uncertainty of the model parameters, as well as the size of the parameter fits.

The solution of equation (1) is given by the conjugate gradient method. The data uncertainty values σ_i are calculated from first-break picks, and the model parameter uncertainty values σ_j are fixed.

A model resolution matrix is also calculated. The diagonal elements of the resolution matrix vary between zero and one and indicate the degree of average or linear dependence of the true model represented by the inverted model. Equivalently, they indicate the relative number of rays that sample each model parameter. Values greater than 0.5 are generally well resolved and reliable.

The method also estimates *a posteriori* model covariance matrix, which can be transformed to standard errors or *a posteriori* model parameter uncertainty. These calculated errors are considered to represent a lower bound of the real parameter errors, as they are due only to the uncertainties of the traveltime picks and do not take into account the trade-offs between the model parameters (Zelt and Smith, 1992). Therefore, calculated error estimates are best used for a relative comparison with the uncertainty estimation from other parameters and also quality control.

REFRATOM

The Refratom program, which performs the *pick* of the first break, calculates the initial model and makes a seismic refraction tomography in 2D and 3D land seismic data. The initial model is constructed by interpreting the cross-over points in the absolute offset domain through the first arrival slopes (it does not consider different sides of the *split-spread* arrangement). The refraction tomography is based on the Amorim *et al.* (1987) algorithm, which considers a single layer over a half-space, i.e., the LVL and refractor. In practice, this implies that all intermediate refractors, before the last one, are part of the LVL, regardless of how many intermediate refractors are considered.

The model parameterization consists of two media divided into vertical prisms of constant velocities; therefore, they can vary only laterally. Each block is of equal horizontal length and has an unknown constant velocity. Figure 2 shows an example of near-surface model parameterization with three layers. The depth (h) and refractor velocity (V_1) are constant, and only the weathering velocity parameter (V_0^*) is estimated. A planar refracting horizon was considered in the original algorithm; however, the algorithm was improved to incorporate a variable refraction depth through an estimate of the initial refractor depth obtained from the delay time method. However, in tomographic inversion, the depth of the refractor is kept fixed, that is, it is not updated.

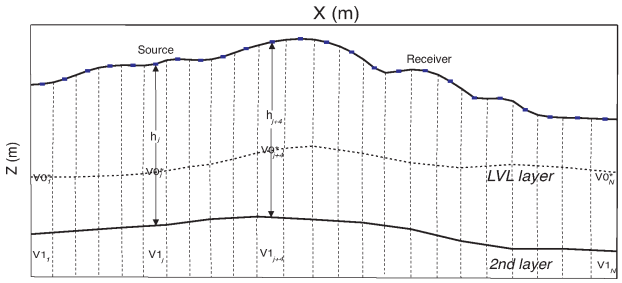

Figure 2. Example of near-surface velocity model parameterization for refraction tomography in Refratom. The three-layer model is reduced for the two-layer model, where the LVL layer is the mean from the first and second layers. The vertical prism has regular width and is centered at the source and receiver locations.

For forward modeling in the tomography algorithm, ray tracing is simpler; rays travel vertically when they leave the source to reach the refractor, then they travel along the surface of the refractor, and finally ascend vertically to the receiver. The algorithm employs a concept called "vertical tomographic velocity" (V_0^*), which has the following relation in Eq. (2) (Amorim *et al.*, 1987):

$$V_0^* = \frac{V_0}{\cos\theta_c} = \frac{V_0 V_1}{\sqrt{V_1^2 - V_0^2}}, \qquad (2)$$

where θ_c is the critical angle.

Equation (2), which relates V_0^* with the true velocity, indicates that it is independent of the thickness of the LVL (Z_1) and dependent only on the velocity propagation in the LVL (V_0) and the underlying rock (V_1). This vertical ray approximation is valid because, in most cases, the LVL is not exceedingly thick and has low velocities (less than 1500 m/s).

The expression for the traveltime of the refracted wave between the points i and j is given by Eq.(3) (Amorim *et al.*, 1987):

$$t_{ij} = \frac{h_i}{V_{0i}^*} + \frac{h_j}{V_{0j}^*} + \sum_{k=1}^{N} \frac{L_{ij}}{V_{1i}}, \quad (3)$$

where:
t_{ij} is the time of the first break (refraction at the base of the LVL) read from the reflection seismogram;
h_i is the LVL thickness at the source i position;
h_j is the LVL thickness at the receiver j position;
V_{0i}^* is the tomographic vertical velocity at the source i position;
V_{0j}^* is the tomographic vertical velocity at the receiver j position;
L_{ij} is the source-receiver distance;
V_{1k} is the refractor's velocity for block k and;
$\sum_{k=1}^{N} \frac{L_{ij}}{V_{1i}}$ is the sum of traveltimes in each block along the LVL base.

Each first break time read in the reflection seismograms will provide an equation. For the various shot and receiver points of the reflection surveys, the first-break traveltime equations represent an over-determined system of equations with unknown V_{0i}^* , V_{0j}^* and V_{1k}, which in matrix notation can be rewritten as — Eq. (4):

$$\mathbf{Ax} = \mathbf{t}, \quad (4)$$

where **A** is the matrix of the ray trajectories, **x** the unknown vector and **t** the vector of the times of the first breaks read in the reflection seismograms.

The system of equation can be solved by least-squares — Eq. (5) (Amorim *et al.*, 1987):

$$\mathbf{x} = [\mathbf{A^T A}]^{-1} \mathbf{A^T t} \quad (5)$$

Due to the sparsity characteristic (large amount of zeros) of matrix **A**, the solution uses the conjugate gradient method.

Although the refractor velocity V_{1k} is also one of the parameters to be determined, according to the (5) system, in practice this value is not inverted due to the instability of the solution. The Refratom program considers fixed values for V_{1k}, not being altered in the tomography (it is estimated by interpretation methods of the *slope* of the refracted waves and later smoothed internally). Before applying tomography, an internal smoothing filter is applied on the refractor velocity V_{1k} to remove anomalous values and attenuate the apparent velocity due to the refractor dip. The equation system also considers fixed values for thickness h_k, which is estimated with delay time methods. Therefore, the program inverts only the *vertical tomographic velocities* V_0^*, which are later converted to the LVL velocity V_0 by the relation (2) and a final thickness h is calculated using the following relation — Eq. (6):

$$h_i = \frac{t_{ii} V_{0i}^*}{2}, \quad (6)$$

where t_{ii} is the intercept time.

Despite the simplicity, the refraction tomography from Refratom represents a good approximation for the traveltime of the refracted waves for LVL situations with an undulated base. It can therefore be used to calculate the refraction traveltime and produce satisfactory results using 2D and 3D land seismic reflection data.

APPLICATION IN REAL DATA

Line L230-401

This seismic line is located in the Potiguar Basin, in the Serra do Mel region, more specifically in the region with the highest topography. Table 3 provides a summary of the acquisition parameters. It is worth mentioning that, in this line, the shot stations are positioned between the receiver stations.

The shallow velocity model for this line consists of an LVL with a vertical velocity gradient and one refractor that varies laterally in velocity. The vertical gradient in LVL allows the propagation of turning-rays. Such a model in this region of the Potiguar Basin has a geological justification. Serra do Mel is composed of the Barreiras formation, which can be divided into unconsolidated sands and, further down, sessions interspersed with clays and sandstones, with a gradual increase in velocity throughout the formation (Maia and Bezerra, 2014). After the Barreiras formation, there are interdigitated sequences of Tibau sandstone and Guamaré carbonate, generating thin layers with higher seismic velocities. Zones with altered carbonate can coexist at the transition interface of the Barreiras and Jandaíra formations, generating higher velocities. In this sense, the LVL in this region is composed of a thick package of sediments that is compact with depth, generating a model with a vertical velocity gradient ranging from 400 m/s to 1000 m/s at the top and reaching 2000 m/s to 2500 m/s at the base. Under the Barreiras is Jandaíra carbonate, with much higher velocities that vary from 4000 m/s to 4500 m/s. The vertical velocity gradient above the Jandaíra favors the propagation of turning-rays in the highest parts of Serra do Mel.

Initial Model Definition

This data have a vertical velocity gradient in the LVL. In the upper part of Figure 3, the T–X graph of shot station 720 (located at X = 11175 m) is shown, with the cross-over points definition, separating the direct wave events, fictitious first refraction layer, and second refraction layer, for each arm of the split-spread arrangement. In the bottom of Figure 3, a T–X graph of all shots and all interpreted cross-over points are shown. The blue and red dots define the cross-over points that separate the direct wave from the first refraction layer and the first from the second refraction layer, respectively.

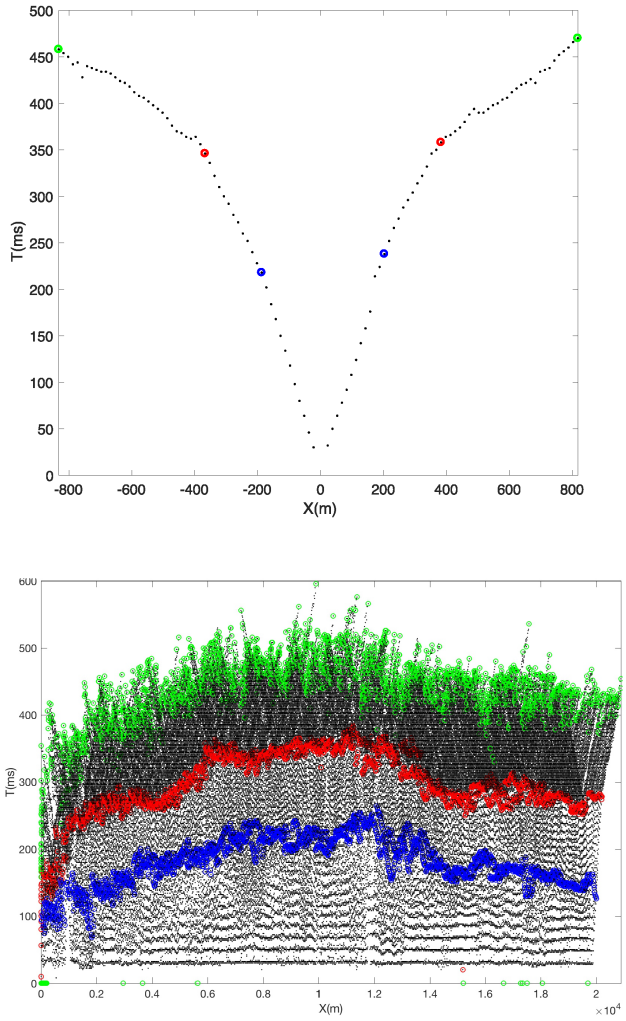

Figure 3. Top: *Cross-over points* from shot 720 (located at X = 11175 m) of line L230-401. Bottom: *cross-over points* from all shots of line L230-401.

Figure 4 shows the velocity V_0 (in red) defined by the average of the velocities of the positive (in blue) and negative (in green) arms. In black, it is possible to compare with the V_0 estimated by Refratom. The velocity V_0 inverted by Refratom is higher and oscillates less than the initial estimated V_0. This is because the Refratom only operates with a two-layer model, so the LVL velocity of this method is essentially the average of the initial V_0 and V_1. To better understand, see Figure 3. In Refratom, V_0 is measured from the origin to the red point; that is, there is no intermediate refractor. Thus, in addition to the higher velocity, it is smoother because it uses more picked points. In addition, the Refratom software has internal smoothing filters that can affect the final tomography result.

Figures 5 and 6 show the definition of the refractor velocities using the direct vs. reverse shot method for the first and second layers, respectively. We compare V_1 (represented by the red curve in the bottom of Fig. 5) with V_0 of the Refratom (in black), which has lower values on average. This occurs as explained in the previous paragraph: Refratom uses a V_0, which is an average of V_0 and V_1. Whereas, for V_2, in Figure 6, both methods estimated velocities with similar values because they used the same offset range to define velocity in the last refractor.

A smoothing filter was then applied using a median of 151 points in V_0, V_1 and V_2. After smoothing the velocities V_0, V_1 and V_2, the depths Z1 and Z2 were estimated by the *Delay Time* method. Then, a median filter with 51 points was applied at depths Z_1 and Z_2 to smooth the relief of the refractor. These intermediate results are not shown to avoid an excessive number of figures.

Inversion Strategy

We used the standard deviations of differences in reciprocal times to define the uncertainties of the picks, and these σ_t standard deviation values were incorporated into the pick file at the tomography entry. A caveat should be clarified at this point: the position of the shooting stations does not coincide with the position of the receiving stations (the shots were made between the receivers) and, to circumvent this problem, it was necessary to consider that the shots are displaced so that the stations coincide, respecting the reciprocity. This adjustment was made only to estimate the uncertainties of the picks and was disregarded in all other stages. For the depth and velocity parameter uncertainties, we defined the constant values as σ_z = 10 m and σ_v = 100 m/s, respectively.

This line model has vertical velocity variation in the LVL, so we considered the velocity of the LVL (V_0) to be V_0up and the velocity of the first refractor (V_1) to be V_0down. Therefore, the tomography model for L230-401 was defined with 140 points in V_0up, V0down, V_1 and Z_1, totaling 560 points of parameter nodes for inversion. The final model has two layers with 1528 blocks in total (1389 in the first and 139 in the second).

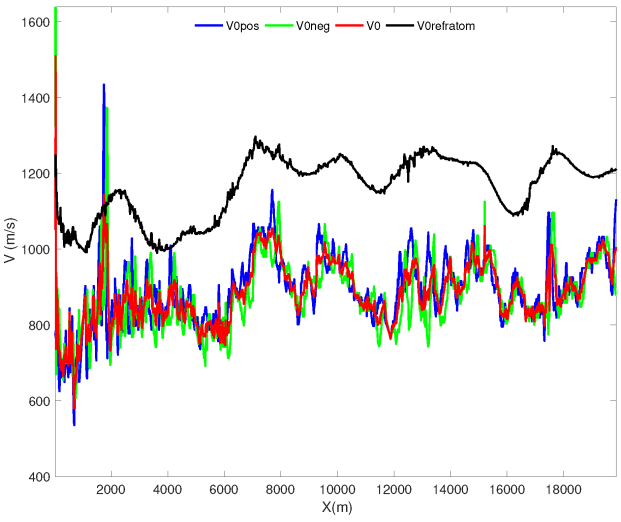

Figure 4. V0 velocity for the positive arm (in blue); for the negative arm (in green); the average value of these velocities used in the initial model (in red); and the Refratom V0 velocity (in black) for lineL230- 401.

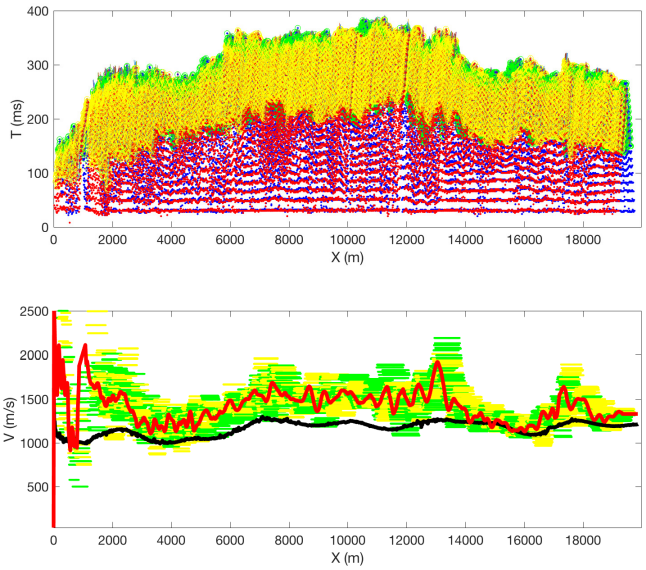

Figure 5. Diagram of the direct vs. reverse shot method - Top: Range of picks used for direct shots (in yellow) and reverse shots (in green). Lower: First refractor (V1) average velocity calculated (red curve) compared to the Refratom V0 velocity (black curve) for line L230-401.

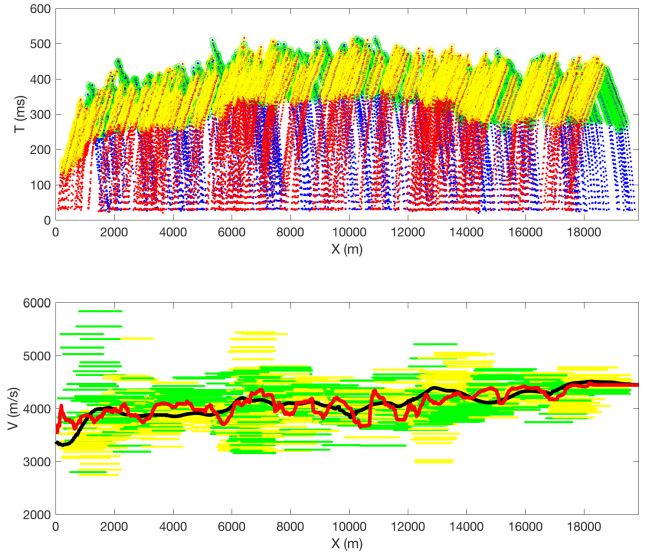

Figure 6. Diagram of the direct vs. reverse shot method - Top: Range of picks used for direct shots (in yellow) and reverse shots (in green). Lower: Second refractor (V2) average velocity calculated (red curve) compared to the Refratom V1 velocity (black curve) for line L230-401.

Results

Table 4 contains several control parameters for the ray tracing and inversion of each iteration. After performing five iterations, a root mean square (RMS) residual traveltime of 6.465 ms and $\chi^2 = 2.613$ were obtained.

Figure 7 shows the graphs of the initial model (blue curve) and the inverted model (red curve) for Z_1, V_0up, V_0down, V_1 and statics corrections at receiver stations. The model generated by the Refratom (green curve) and the depth of the top of the Jandaíra formation from four wells projected on the line are also shown. The final inverted model became deeper, by approximately 50 m, in relation to the initial and Refratom models. The initial and inverted V_0up were similar; however, the V_0down increased significantly (from approximately 1500 m/s to 2500 m/s). This increase in V0down only occurred because of the presence of turning-rays in the model with a vertical velocity gradient. The refractor velocity, V1, did not change significantly (remaining between 4000 m/s and 4500 m/s). The statics corrections were calculated at the receiver stations and depth 0 m.

Figure 8 shows the resolution and covariances *a posteriori* for velocities (V_0up, V_0down and V_1) and depth (Z_1). There was a higher resolution for V0up and similar values for V0down and V1 (around 0.4), and a higher uncertainty for V_0down and V_1 (approximately 80 m/s) and a lower one for V_0up (approximately 40 m/s). This discrepancy happens because there are more turning-ray arrivals in relation to total refraction rays (comparison of the green and red rays). Because the turning-rays cannot reach the bottom of the layer completely, the resolution of V_0down is lower than that of V_0up. The covariances are the resolution inverse response, and, as expected, the uncertainty is higher in the lower resolution and low coverage region. For all of them, the boundary effect is evident because of the reduced coverage of the rays.

Figure 9 shows, in the upper part, the ray-tracing diagram derived from the final inverted model and the respective T_X graph with the real picks and those calculated by refractive tomography for shots located at X = 1080 m, 5400 m, 8160 m, 11010 m, 14280 m and 18390 m; and in the bottom, a zoom of the ray trace diagram and T–X graph for the shot located at X = 11000 m. The good correlation between the actual and inverted traveltimes for all arrivals is noticeable. The curved effect of turning-rays (red color) and *head-waves* (green color) when propagating in the layer with vertical velocity gradient is also evident. This shows that the approximation of straight-rays does not represent well models with vertical velocity variation.

Figure 10 shows, respectively, the seismograms from shot station 1181 with first break picks and without statics, with statics from the Rayinvr model and with statics from the Refratom model (both located in the floating *datum*). Due to the low signal-to-noise ratio and little topographical variation, it is not possible to observe changes in reflections in this domain.

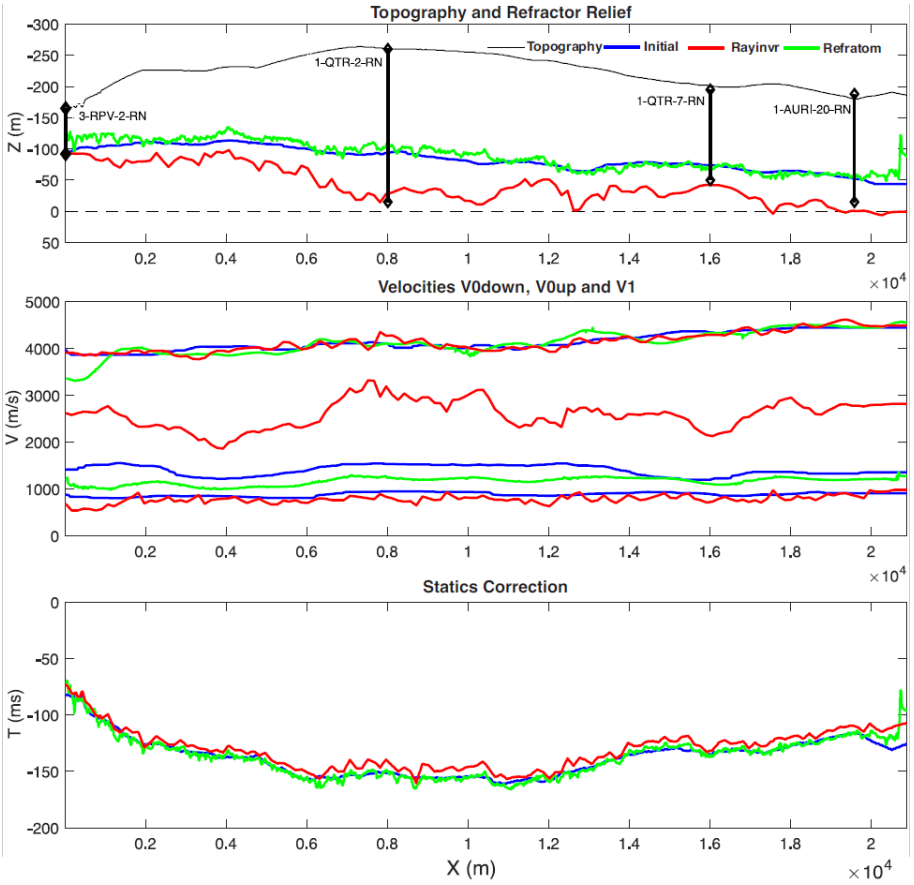

Figure 7. Real (black line), initial (blue line), inverted by Rayinvr (red line) and inverted by Refratom (green line) models from line L230-401. For initial and Rayinvr models, the same colored lines represent the velocities V0up, V0down and V1 (bottom-up direction) in the middle graph. For Refratom model, the same colored lines represents V0 and V1 in the middle graph.

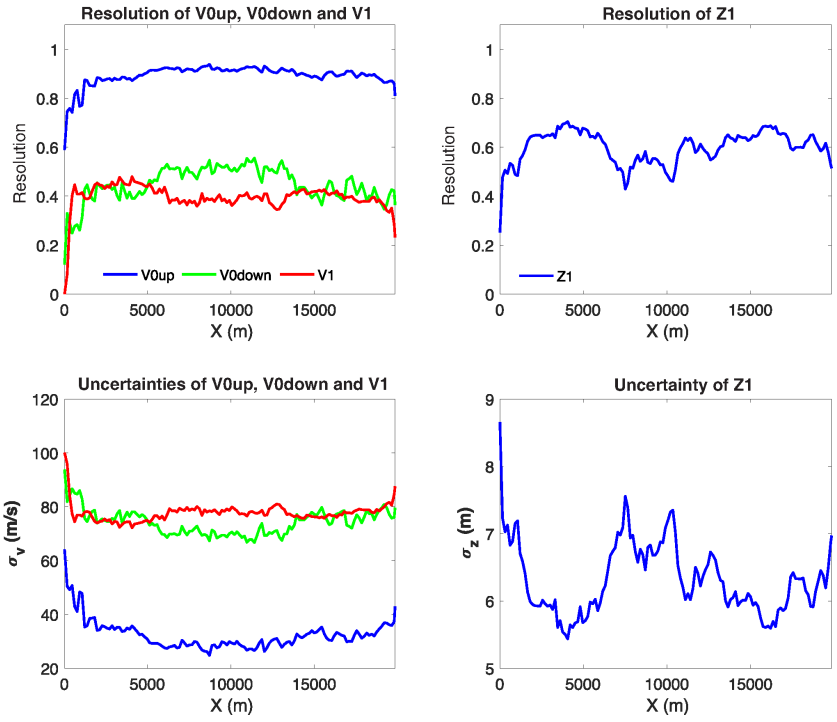

Figure 8. Resolution and Uncertainties (*Posteriori* Covariance) for line L230-401.

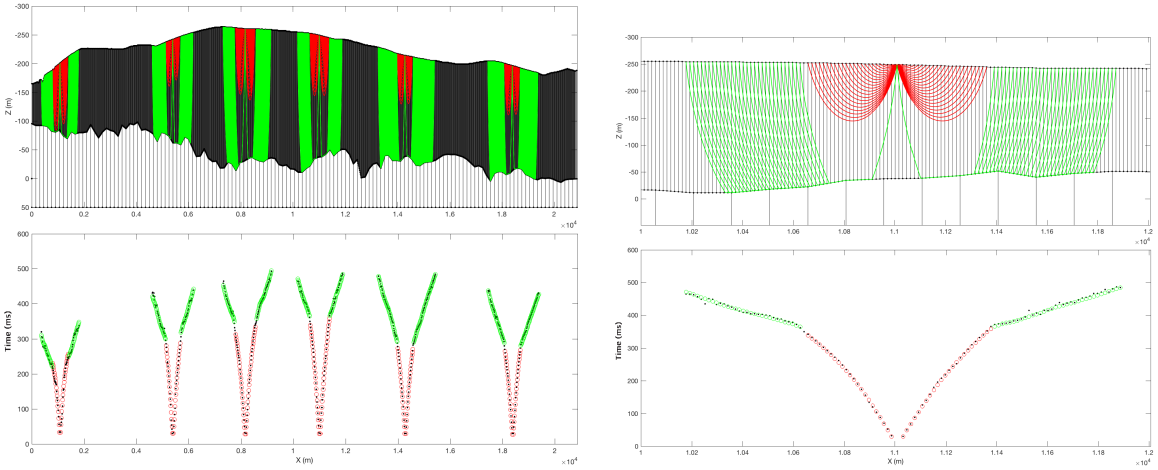

Figure 9. Top: Ray diagram (above) and T-X graph (below) of five shot points, located at X = 1040, 2080, 4000, 5440 and 7040 m of line L230-401. Bottom: Ray diagram (above) and T–X graph (below) of the zoom-in of region X = 11000 m. The colors show rays and traveltime of turning-rays on the first layer (red) and refraction on the second layer (green).

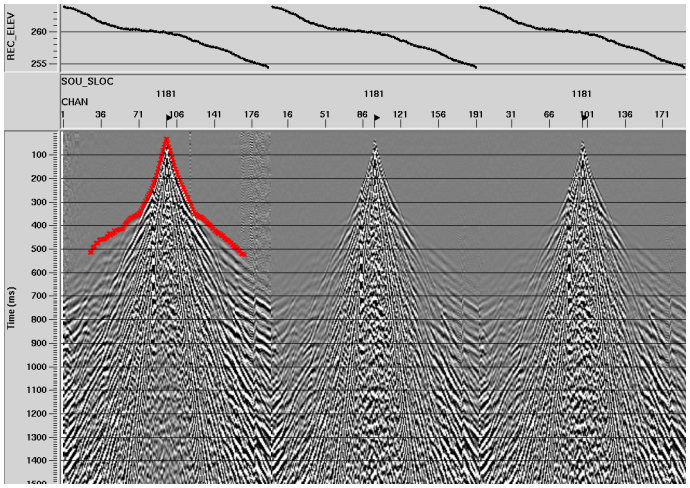

Figure 10. Seismogram from shot station 1181 for line L230-401. From left to right: (a) with first break picks and no statics, (b) with statics from the Rayinvr model and (c) with statics from the Refratom model. Statics corrected shots are located in the floating *datum*. The graphic in the top shows the topography of the receiver.

Table 2. Well locations and refractor's depth (top of Jandaíra Formation) for the wells, Rayinvr (showed as Ray subscript) and Refratom (showed as Ref subscript) inversions for line L230-401. Coordinate System in UTM MC 39 W SIRGAS-2000.

Well	X	Y	Z_{Well}	Z_{Ray}	Z_{Ref}	ΔZ_{Ray}	ΔZ_{Ref}
3-RPV-2-RN	702410.4	9417763.3	-91.95	-95.35	-122.80	-3.40 m	-30.85 m
1-QTR-2-RN	708672.6	9424801.0	-15.00	-28.55	-106.5	-13.55 m	-91.50 m
1-QTR-7-RN	717199.7	9424989.3	-49.93	-41.99	-66.40	+7.94 m	-16.47 m
1-AURI-20-RN	719838.5	9429061.9	-15.00	-0.69	-53.80	+14.31 m	-38.80 m

Figure 11 shows the stacked seismic section after the statics correction for (a) the initial, (b) Rayinvr and (c) Refratom models, respectively. For all sections, poor seismic quality can be observed, which is very common in most of the seismic data in the Serra do Mel region. However, there were regions with improvement and others with worsening in the alignment of the shallower reflector, which follows the topography and general improvements of some reflection events, such as those between CDPs 222 and 882 at the times of 300 ms and 400 ms (shown in the figure as red arrows). The stacked section with the inverted model became slightly deeper in time (about 20 ms) compared to the initial and Refratom models (showed in the figure as yellow arrows). This is because the statics correction, as observed in Figure 7, was slightly less than in the initial and Refratom models. A more or less constant temporal shift (+20 ms) can compromise locations and time-depth conversion steps.

The general result of this inversion was satisfactory and managed to optimize the shallow velocity model parameters, obtaining lower RMS error values than the initial model. The depth found in the refractor approaches the top of the Jandaíra formation observed in the wells of Figure 7, validating a velocity model with a vertical gradient of velocities in the LVL. Table 2 summarizes well locations, the depth of the refractor (top of the Jandaíra formation) from wells and Rayinvr results, and the difference between inverted and wells. The differences were much smaller for the Rayinvr inversion.

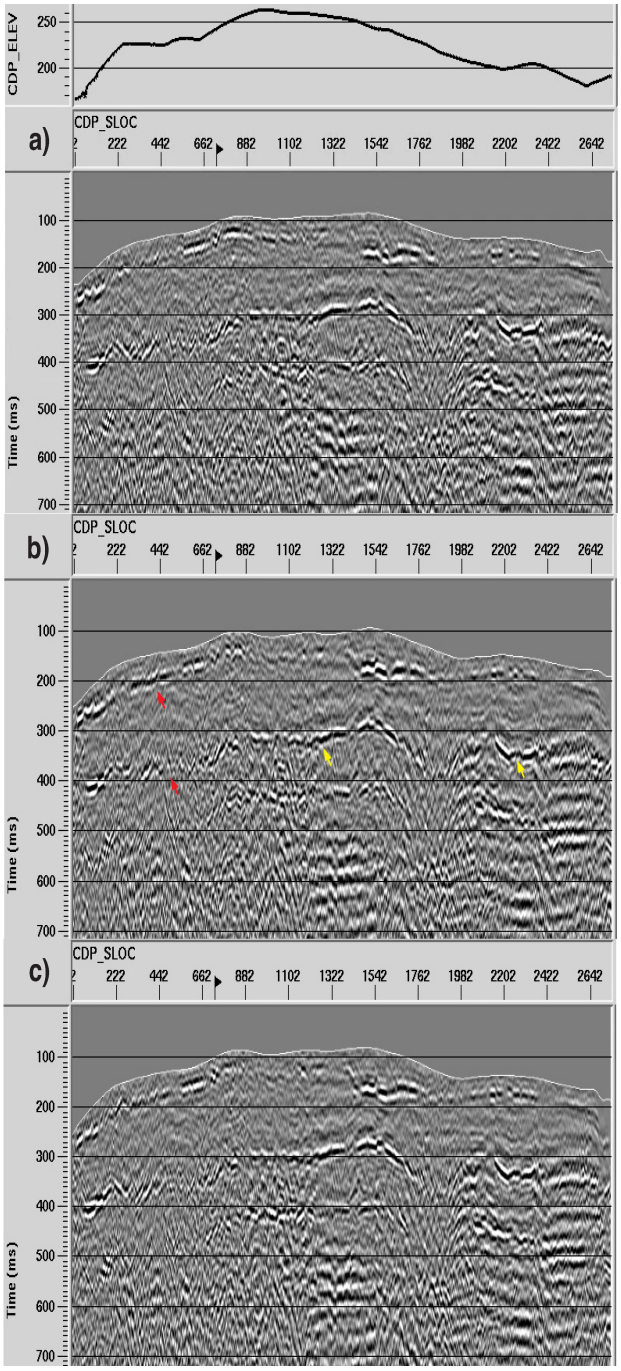

Figure 11. Stacked sections of the L230-401 seismic line from Potiguar Basin, with statics correction from: (a) initial model, (b) Rayinvr model and (c) Refratom model. The red arrows show a better definition of shallow reflectors, and the yellow arrows show a time shift of approximately +20ms.

Line L319-024

This seismic line is located in the Paraná Basin, an onshore Brazilian sedimentary basin considered a new exploration frontier. This line was acquired with a Vibroseis type font with geometry in crooked format. Table 5 provides a summary of the acquisition parameters.

The shallow velocity model for this line consists of one LVL and two refractors. The shallow part has a sedimentary cover of the Bauru formation, composed of continental siliciclastic sediments from wind, fluvial, and alluvial systems. It is located below the Serra Geral formation, composed of basaltic spills that cover the entire Paraná Basin (Milani *et al.*, 2007). Owing to this formation of magmatic origin, a large part of the seismic energy cannot propagate beyond it (some places have layered packages with up to 2000 m of basalt over the sediments of the Paraná Basin, in addition to intrusions between them, in the form of dikes and thresholds). The weathered layers form the LVL, with velocities around 700 m/s to 1200 m/s. Below this layer it comes the Bauru formation, which forms a first refractor with velocities around 1800 m/s to 2400 m/s. Then, the Serra Geral formation would occur, forming a second refractor with very high velocities, around 4800 m/s to 5200 m/s.

Initial Model Definition

In the upper part of Figure 12 the T–X graph of shot station 775 (located at X = 41750 m) is shown, with the *cross-over points* definition, separating the direct wave events, the first and second layer refraction, for each arm of the split-spread arrangement. In the bottom of Figure 12, a T–X graph of all shots is shown, and inter-

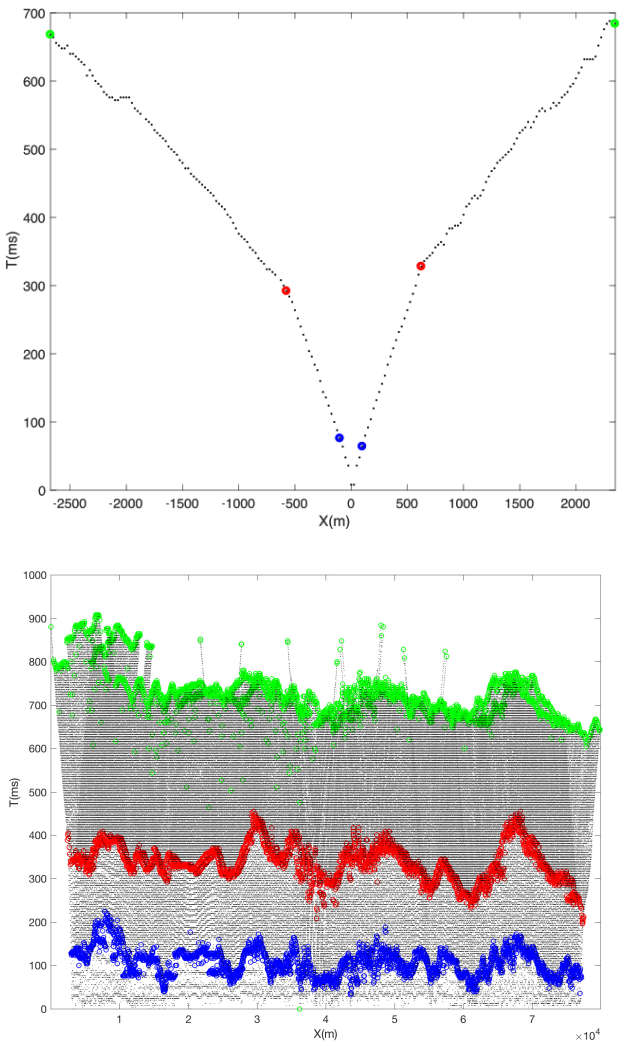

Figure 12. Top: Picks from first break (black) and the *cross-over points* (red, blue and green) for shot 775 (located at X = 41750 m) of line L319-024. Bottom: Picks from first break (black) and *cross-over points* (red, blue, and green) from all shots of line L319-024.

preted *cross-over points*. The blue and red dots define the *cross-over points* that separate the direct wave from the first refraction layer and the first from the second refraction layer, respectively. The green dot defines the last point definition of the second layer refraction event.

With the *cross-over points*, the initial velocities V_0, V_1 and V_2 were estimated using the same methodology used to previous line. To remove unwanted variations, we smoothed the result velocities by applying a median filter of 101 points for V_0 and V_1, and 301 points for V_2. Then, we calculated the depths Z_1 and Z_2 using the *Delay Time* method and, finally, we applied a median filter with 151 points to remove anomalous values.

Inversion Strategy

To define the uncertainties of the picks, we used the standard deviations of differences in reciprocal times, and these σ_t standard deviation values were incorporated into the pick file at the tomography entry. For the depth and velocity parameter uncertainties, we defined the constant values as σ_z = 10 m and σ_v = 100 m/s, respectively.

The tomography model for L319-024 was defined with 320 points in V_0, V_1 and V_2, Z_1 and Z_2, totaling 1600 points of parameter nodes for inversion. The final model has four layers with 7016 blocks in total (3189 in the first, 3189 in the second, 319 in the third, and 319 in the fourth).

Initially, we followed a layer stripping strategy, first resolving V_0, then V_1 and Z_1, then V_2 and Z_2. Finally, all parameters were inverted. However, there was a formation of anomalous regions, mainly for V_2 and Z_2. To solve this problem, we performed a complete inversion of all parameters from the beginning, inverting V_0, V_1 and V_2, Z_1 and Z_2 simultaneously. In the end, we noticed the same anomaly formation for V_2 and Z_2.

After an analysis, we realized that the problem was not in the inversion, but in the geometry of the acquisition line. The line has a crooked geometry, as shown in Figure 16, and therefore, the time-distance curves do not represent seismic events located in the 2D plane of the source-receiver. As the tomography algorithm used does not consider azimuths of ray propagation, that is, only strictly 2D events, the inversion of parameters that deviate from the source-receiver plane generates distortions in the inverted parameters.

RESULTS

Table **??** contains several control parameters for the ray tracing and inversion for each iteration of the Rayinvr tomographic inversion. After performing seven iterations, a RMS residual traveltime of 8.851 ms and $\chi^2 = 2.914$ was obtained.

Figure 13 shows the graphics of the initial model (blue curve) and inverted by Rayinvr (red curve) model for the relief of the Z_1 and Z_2 refractors, V_0, V_1 and V_2 velocities and statics corrections at the receiver stations. The model was generated by Refratom (green curve), with Z_2 refractor depth and V_0 and V_2 velocities. The regions near stations X = 38000 m, 55000 m, and 61000 m showed abrupt increases in velocity V_2 and depth Z_2 that, as we discussed earlier, are associated with the crooked geometry acquisition (as shown in Figure 16, with warm colors showing regions with a change in acquisition geometry). Statics correction values were calculated for a fixed *datum* of 1200 m above sea level, with a fixed replacement velocity equal to 4800 m/s (which is an average of V_2 and is necessary for *datums* above sea level).

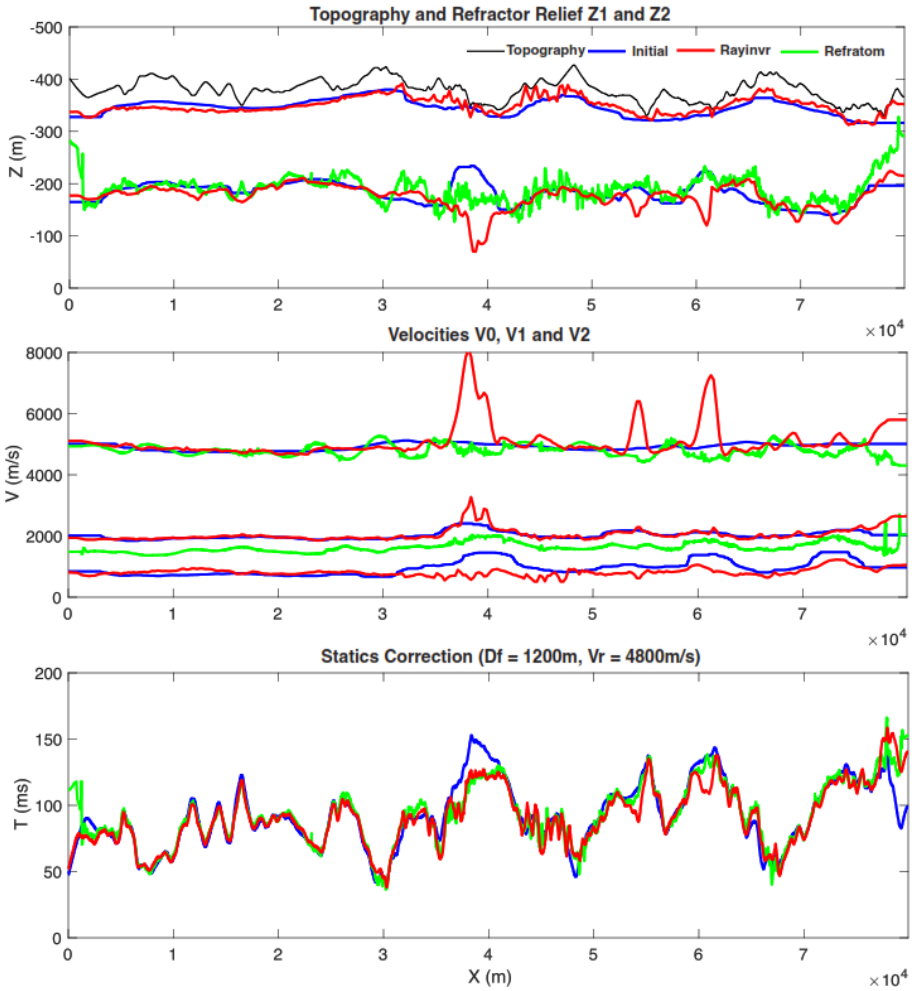

Figure 13. Models from line L319-024: real (black line), initial (blue line), inverted by Rayinvr (red line) and inverted by Refratom (green line). For initial and Rayinvr models, the same colored lines represent the depths of the refractors Z1 and Z2 in the top graph, and the velocities V0, V1 and V2 (bottom-up direction) on the middle graph. For Refratom model, the same colored lines represent V0 and V1 in the middle graph.

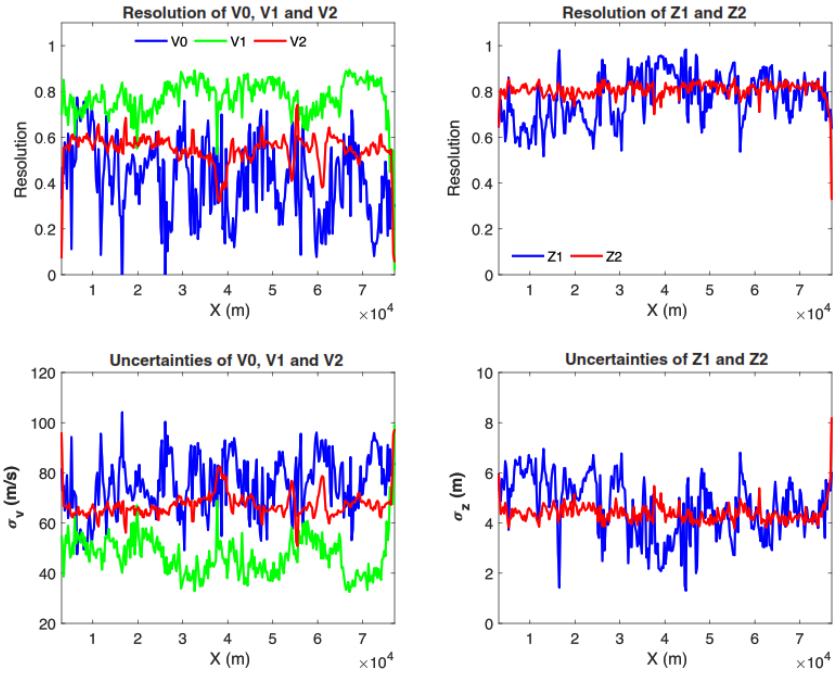

Figure 14. Resolution and Uncertainties (*Posteriori* Covariance) for model from line L319-024.

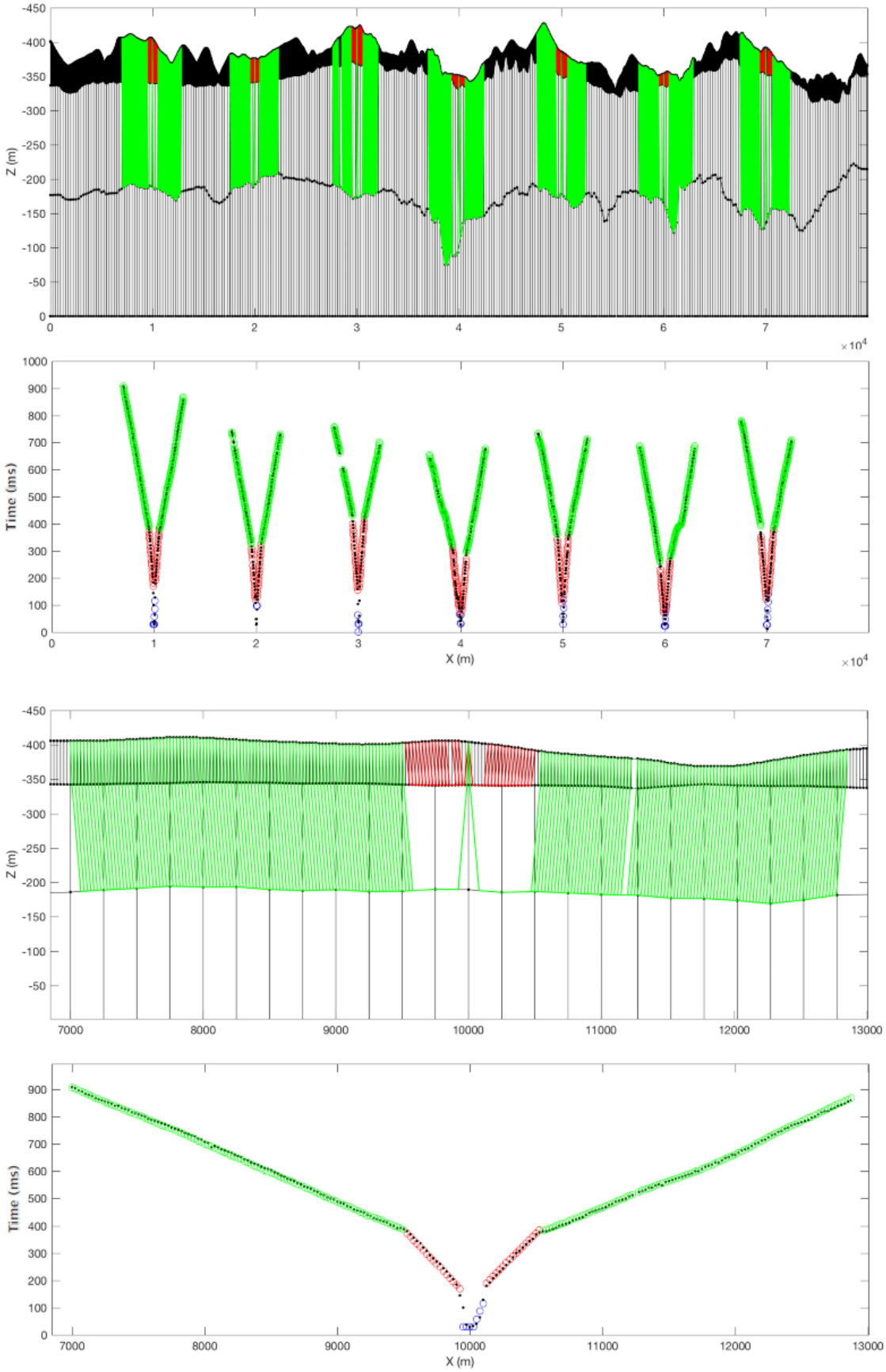

Figure 15. Top: Ray diagram (above) and T-X graph (below) of five shot points, located at X = 6000, 10000, 14000, 18000 and 21200 m of the line L319-024 model. Bottom: Ray diagram (above) and T-X graph (below) of the zoom-in of region X = 10000 m. The colors show rays and traveltimes of turning-rays on the first layer (red) and refraction on the second layer (green).

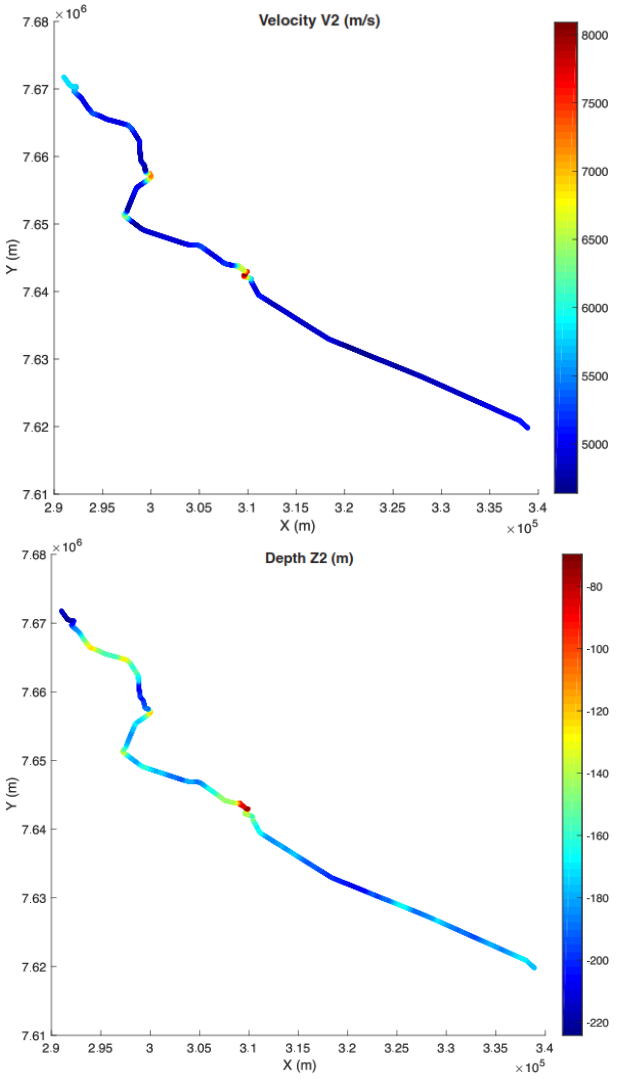

Figure 16. Map representation of the inverted velocity V2 (top) and depth Z2 (base) of line L319-024. Note that the anomalous regions generated in the inversion are located in the parts where the major source-receiver direction changes in the *crooked* line occur, as shown in Figure 13.

Figure 14 brings the resolution and covariance graphs to *posteriori* of velocities (V_0, V_1 and V_2) and depths (Z_1 and Z_2). The resolution of V_0 has high frequency and strong variation owing to the very low coverage of the *picks* in this range. The resolution of V_1 was more stable, with values close to 0.8. The V_2 resolution was also stable at approximately 0.6, but with some positions reaching 0.4 (precisely in regions with anomalous V_2 values as previously described). The resolution of Z_1 had a greater oscillation than the resolution of Z_2, but both were, in general, above 0.7.

Figure 15 shows, in the upper part, the ray-tracing diagram made in the final inverted model and the respective TX graph with the real picks and those calculated by refraction tomography for shots located at X = 10000 m, 20000 m, 30000 m, 40000 m, 50000 m, 60000 m, and 70000 m; and in the bottom, a zoom of the ray trace diagram and T–X graph for the shot located at X = 10000 m. There was a good correlation between the actual and inverted traveltimes for all arrivals.

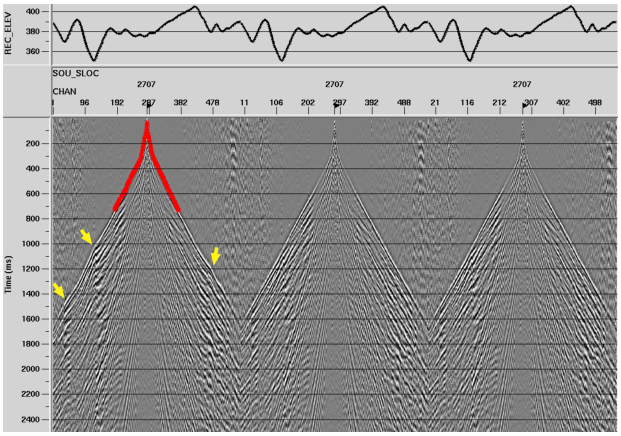

Figure 17. Seismogram from shot station 2707 of line L319-024. From left to right: (a) with first break picks and no statics, (b) with statics from the Rayinvr model and (c) with statics from the Refratom model. Statics corrected shots are located in the floating *datum*. The yellow arrows show regions of greater statics influence (corrected by both tomography methods). The graphic in the top shows the topography of the receiver.

Figure 17 shows, respectively, the seismograms from shot station 2707 with first break picks and without statics, with statics from the Rayinvr model and with statics from the Refratom model (located in the floating *datum*). The yellow arrows highlight major changes in reflections due to strong topographical variations.

Figure 18 shows the stacked section after the static correction for the (a) initial model, (b) inverted by Rayinvr, and (c) Refratom model. The seismic input data had F–K filtering in the shot and receiver domain and automatic-gain control before stacking. Comparing 18(a) and 18(c), it is clear that the best alignment of the reflectors for inverted model by Rayinvr. In 18(b), analyzing a white peak reflector slightly below 400 ms, in the vicinity of CDP 3951 and 4473, it is possible to notice a *pull-up* (indicated by the red arrows in the figure). This temporal distortion is because of the crooked geometry of the line, which, as we have already explained, generated anomalous values for V_2 and Z_2. Comparing Figures 18(b) and 18(c), we noticed a greater lateral oscillation in several reflectors in the Refratom model along the entire line (showed in the figure as yellow arrows). These temporal distortions were not expected outside the crooked regions, and therefore we consider the data stacked by the Rayinvr inversion model to be more reliable.

Line L319-024 is located in an oil exploration frontier region and, unlike L230-401, there is no well close to it that can be used as a geology control. Despite this, the overall inversion result was satisfactory and constrained the parameters of the shallow velocity model, resulting in lower RMS error values than in the initial model.

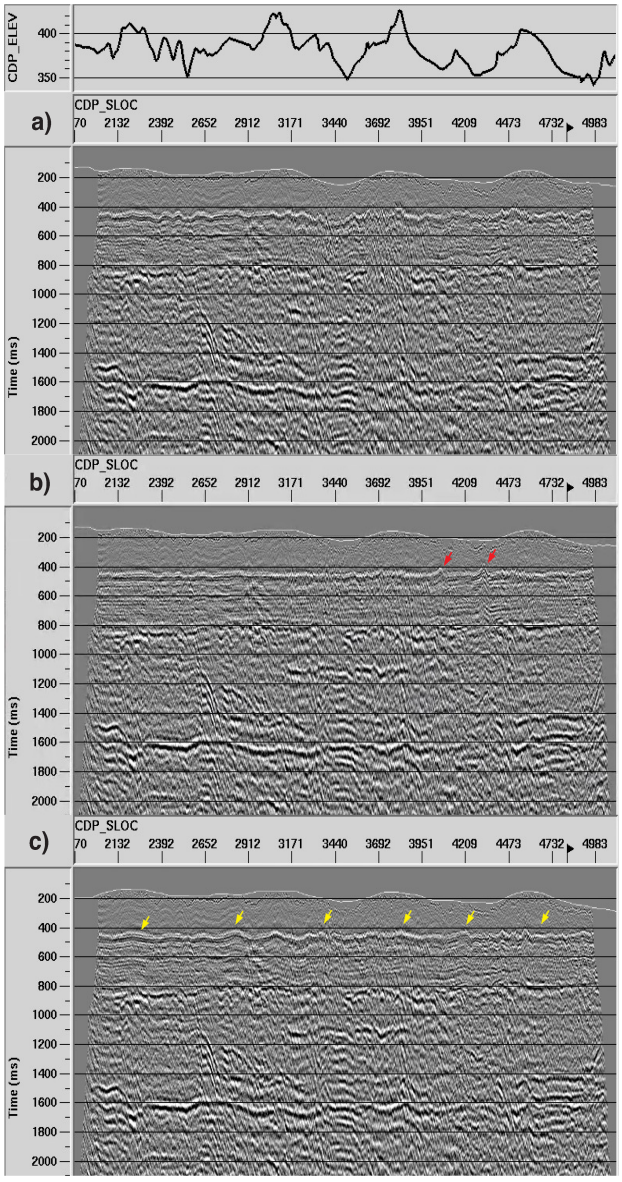

Figure 18. Stacked sections of the L319-024 seismic line from Paraná Basin, with statics correction from: (a) initial model, (b) Rayinvr model and (c) Refratom model. The red arrows show pull-ups because of the crooked geometry, and the yellow arrows show abnormal oscillatory on reflectors for the Refratom model.

The depth model obtained has three layers, unlike Refratom. Even with the problems due to crooked acquisition, compared to the initial and Refratom models, the stacked section by the inverted model with Rayinvr provides lower lateral oscillations of the reflectors, which affords greater confidence for processing in time.

CONCLUSIONS

The Rayinvr tomography algorithm, commonly used for crustal studies, has been successfully adapted and applied to real data from two seismic lines in Brazilian terrestrial basins, acquired for oil exploration. This algorithm provided good quality and geologically consistent results of the near-surface layered structure and also of the velocity model of terrains with rough topography. Its results are more accurate than those obtained by the Refratom tomography algorithm widely used in the industry.

For line L230-401, the final inverted structural model has the refractor depth closest to the depths found by the wells available in the area, which validates the reliability of the results of the inversion with Rayinvr when compared with the initial and Refratom models. In addition, the refraction tomography's joint inversion of turning-rays and head-wave events proved to be reliable and provided a geologically consistent LVL model.

For line L319-024, Rayinvr provided the LVL model formed by two refractors and three refractors, which allowed us to calculate better static corrections that result in stacked data with much less oscillations than in the initial and Refratom models. This result demonstrates that the Rayinvr also provides a satisfatory LVL velocity model in areas with sedimentary and igneous occurrences near the surface, as in line L319-024.

The objective of the work was achieved, being possible to apply and analyze the results in two 2D land seismic reflection data. It was observed that for regions with strong changes in the source-receptor azimuth, the Rayinvr inverted values for refractor velocity and depth were locally anomalous. Complementary studies must be conducted to deal with situations where seismic events leave the 2D plane (situations with crooked geometry and 3D acquisitions).

Despite that, the velocity models obtained with the proposed inversion strategy are more accurate than those obtained with the standard algorithm. Therefore, they can be applied with confidence for statics corrections, prestack data redatuming, and depth imaging from topography.

ACKNOWLEDGMENTS

The authors would like to thank PETROBRAS for support and permission to use the Refratom software, ANP for release and permission to use seismic and well data, UFRN/PPGCEP for the infrastructure, and Colin A. Zelt for making the codes available and for his assistance in the parameterization of Rayinvr.

APPENDIX

Table 3. Acquisition parameters for line L230-401.

Parameter	Value
Acquisition Year	1987
Source Type	Explosive
Sample Rate	2 ms
Register Time	4 s
Total Shot Point	1285
Number of Channels	192
Total Station Points	1421
Total Traces	241847 (147722)
Station Interval	7.5 m
Shotpoint Interval	7.5 m
Range	2350–150–0–150–2350 m
Line Extension	21255 m

Table 4. Line L230-401: tomography results for Rayinvr.

Parameter	it0	it1	it2	it3	it4	it5
Total Rays Traced	553437	568110	570645	570515	569841	569280
Total Points on Rays	175352293	26877381	282207373	27723774	27482753	27423065
N. of Traveltime Picks	140244	145058	145429	145393	145341	145264
N. of Parameters to Invert	560	560	560	560	560	560
RMS Residual Traveltime (ms)	21.179	23.014	10.302	7.838	6.641	6.465
χ^2 Normalized	28.033	33.102	6.634	3.840	2.757	2.613
Factor λ	0.1	0.01	0.005	0.0025	0.00125	-
Variance σ_v (m/s)	100 m/s	100 m/s	100 m/s	100 m/s	100 m/s	-
Variance σ_z (m)	10 m	10 m	10 m	10 m	10 m	-

Table 5. Acquisition parameters for line L319-024.

Parameter	Value
Acquisition Year	2009
Source type	Vibroseis
Sample Rate	4 ms
Register Time	5 s
Total Shot Point	1482
Number of Chanels	560
Total Station Points	3212
Total Traces	824957
Station Interval	25 m
Shotpoint Interval	25 m
Range	2350–150–0–150–2350 m
Line Extension	80300 m

Table 6. Line L319-024: tomography results for Rayinvr.

Parameter	it0	it1	it2	it3	it4	it5	it6	it7
Total Rays Traced	703346	703134	703488	703551	703609	704254	705193	706266
Total Points on Rays	60619621	61114877	60600873	60592779	60589072	60615387	60632965	60645558
N. of Traveltime Picks	289116	288648	288350	288103	287082	288360	289435	289946
N. of Parameters to Invert	1600	1600	1600	1600	1600	1600	1600	1600
RMS Residual Traveltime (ms)	19.767	14.935	12.122	10.776	10.214	9.242	8.960	8.851
χ^2 Normalized	21.491	11.664	7.218	5.251	4.418	3.525	3.124	2.914
Factor λ	0.01	0.01	0.01	0.01	0.001	0.001	0.001	-
Variance σ_v (m/s)	100 m/s	100 m/s	100 m/s	100 m/s	100 m/s	100 m/s	100 m/s	-
Variance σ_z (m)	10 m	10 m	10 m	10 m	10 m	10 m	10 m	-

REFERENCES

Amorim, W.; Hubral, P.; Tygel, M. Computing field statics with the help of seismic tomography. *Geophysical Prospecting* **1987**, *35*, 907–919.

Bauer, K.; Neben, S.; Schreckenberger, B.; Emmermann, R.; Hinz, K.; Fechner, N.; Gohl, K.; Schulze, A.; Trumbull, R.B.; Weber, K. Deep structure of the Namibia continental margin as derived from integrated geophysical studies. *Journal of Geophysical Research: Solid Earth* **2000**, *105*, 25829–25853.

Boehm, G.; Francese, R.; Giorgi, M. Integrated Refraction Seismics and Tomographic Study of a Gravitational Collapse Phenomenon. *Bollettino di Geofisica Teorica ed Applicata* **2012**, *53*, 539–550. 10.4430/bgta0081.

Cerveny, V.; Molotkov, I.; Psencik, I. Ray Method in Seismology. *Charles University* **1977**. 215pp.

Dean, S.M.; Minshull, T.A.; Whitmarsh, R.B.; Louden, K.E. Deep structure of the ocean-continent transition in the southern Iberia Abyssal Plain from seismic refraction profiles: The IAM-9 transect at 40 degree 20N. *Journal of Geophysical Research: Solid Earth* **2000**, *105*, 5859–5885. 10.1029/1999jb900301.

Gonçalves, B.F.; Garabito, G. Flexible layer-based 2D refraction tomography method for statics corrections. *Journal of Applied Geophysics* **2021**, *185*, 104254. 10.1016/j.jappgeo.2021.104254.

Gutscher, M.A.; Malod, J.; Rehault, J.P.; Contrucci, I.; Klingelhoefer, F.; Victor, L.M.; Spakman, W. Evidence for active subduction beneath Gibraltar. *Geology* **2002**, *30(12)*, 1071–1074. 10.1130/0091-7613(2002)030<1071:efasbg>2.0.co;2.

Hampson, D.; Russell, B. First-break interpretation using generalized linear inversion. *Journal of the Canadian Society of Exploration Geophysicists, CSEG,* **1984**, *20*, 45–54.

Liu, H.; Zhou, H.; Liu, W.; Li, P.; Zou, Z. Tomographic velocity model building of the near surface with velocity-inversion interfaces: A test using the Yilmaz model. *GEOPHYSICS* **2010**, *75*, U39–U47.

Luo, Y.; Schuster, G.T. Wave-equation traveltime inversion. *GEOPHYSICS* **1991**, *56*, 645–653.

Maia, R.P.; Bezerra, F.H.R. Inversão Neotectônica do Relevo na Bacia Potiguar, Nordeste do Brasil. *Revista Brasileira de Geomorfologia* **2014**, *15*.

Marsden, D. Static corrections: a review, Part 1. *The Leading Edge* **1993**, *12*, 43–49. 10.1190/1.1436912.

Milani, E.J.; H., M.J.; Souza, P.A.; Fernandes, L.A.; B, F.A. Bacia do Paraná. *Boletim de Geociências da Petrobras* **2007**, *15*, 265–287.

Ogunsuyi, F.O.; Schmitt, D.R., 22. Integrating Seismic-Velocity Tomograms and Seismic Imaging: Application to the Study of a Buried Valley. In *Advances in Near-surface Seismology and Ground-penetrating Radar*; 2012; pp. 361–378. 10.1190/1.9781560802259.ch22.

Olsen, K.B. A Stable and Flexible Procedure for the Inverse Modelling of Seismic First Arrivals. *Geophysical Journal International* **1989**, *37*, 455–465.

Pyun, S.; Shin, C.; Min, D.J.; Ha, T. Refraction traveltime tomography using damped monochromatic wavefield. *GEOPHYSICS* **2005**, *70*, U1–U7. 10.1190/1.1884829.

Schuster, G.T.; Quintus-Bosz, A. Wavepath eikonal traveltime inversion: Theory. *GEOPHYSICS* **1993**, *58*, 1314–1323. 10.1190/1.1443514.

Shen, X. Near-surface velocity estimation by weighted early-arrival waveform inversion. *SEG Technical Program Expanded Abstracts 2010* **2010**, pp. 1975–1979. 10.1190/1.3513230.

Sheng, J.; Leeds, A.; Schuster, M.B.G.T. Early arrival waveform tomography on near-surface refraction data. *GEOPHYSICS* **2006**, *71*, U47–U57. 10.1190/1.2210969.

Sheriff, R.E.; Geldart, L.P. *Exploration Seismology, vol 2: Data Processing and Interpretation*; Cambridge University Press, 1983. 240pp.

Stefani, J.P. Turning-ray tomography. *GEOPHYSICS* **1995**, *60*, 1917–1929. 10.1190/1.1443923.

Talukdar, K.; Behera, L. Sub-basalt Imaging of Hydrocarbon-Bearing Mesozoic Sediments Using Ray-Trace Inversion of First-Arrival Seismic Data and Elastic Finite-Difference Full-Wave Modeling Along Sinor–Valod profile of Deccan Syneclise, India. *Pure and Applied Geophysics* **2018**, *175*, 2931–2954. 10.1007/s00024-018-1831-z.

Zelt, C.A.; Ellis, R.M. Practical and efficient ray tracing in two-dimensional media for rapid traveltime and amplitude forward modeling. *Canadian Journal of Exploration Geophysics* **1988**, *24*, 16–31.

Zelt, C.A.; Smith, R.B. Seismic traveltime inversion for 2-D crustal velocity structure. *Geophysical Journal International* **1992**, *108*, 16–34. 10.1111/j.1365-246x.1992.tb00836.x.

Zhou, H.; Li, P.; Yan, Z.; Liu, H. Constrained deformable layer tomostatics. *GEOPHYSICS* **2009**, *74*, WCB35–WCB46. 10.1190/1.3211109.

Zhou, H. Multiscale deformable-layer tomography. *GEOPHYSICS* **2006**, *71*, R11–R19. 10.1190/1.2194519.

Zhu, X.; Sixta, D.P.; Angstman, B.G. Tomostatics: Turning-ray tomography plus static corrections. *The Leading Edge* **1992**, *11*, 15–23. 10.1190/1.1436864.

B.F.G.: conceptualization, methodology, application, writing; **G.G.:** data curation, supervision, editing.

Received on December 20, 2021/ Accepted em May 12, 2022.

-Creative Commons attribution-type BY